Biodistribution studies of ultrasmall silicon nanoparticles and carbon dots in experimental rats and tumor mice

Licciardello, N.; Hunoldt, S.; Bergmann, R.; Singh, G.; Mamat, C.; Faramus, A.; Ddungu, J. L. Z.; Silvestrini, S.; Maggini, M.; de Cola, L.; Stephan, H.;

Originally published:

May 2018

Nanoscale 10(2018), 9880-9891

DOI: https://doi.org/10.1039/C8NR01063C

Nanoscale

PAPER

Biodistribution studies of ultrasmall silicon nanoparticles and carbon dots in experimental rats and tumor mice

Received 5th February 2018,
Accepted 27th March 2018

rsc.li/nanoscale

Nadia Licciardello[1,2,3#], Sebastian Hunoldt[1#], Ralf Bergmann[1], Garima Singh[1], Constantin Mamat[1], Angélique Faramus [2,3], John L. Z. Ddungu [2,3], Simone Silvestrini[4], Michele Maggini[4], Luisa De Cola [2,3*] and Holger Stephan[1*]

Ultrasmall clearable nanoparticles possess enormous potential as cancer imaging agents. In particular, biocompatible silicon nanoparticles (Si NPs) and carbon quantum dots (CQDs) hold great potential in this regard. Their facile surface functionalization easily allows the introduction of different labels for *in vivo* imaging. However, to date, a thorough biodistribution study by *in vivo* positron emission tomography (PET) as well as a comparative study of Si *vs* C particles of similar size are missing. In this contribution, ultrasmall (size < 5 nm) Si NPs and CQDs were synthesized and characterized by high-resolution transmission electron microscopy (HR-TEM), Fourier-transform infrared (FTIR), absorption and steady-state emission spectroscopy. Subsequent functionalization of NPs with a near-infrared dye (Kodak-XS-670) or a radiolabel (^{64}Cu) enabled a detailed *in vitro* and *in vivo* study of the particles. For radiolabeling experiments, the bifunctional chelating agent *S*-2-(4-isothiocyanatobenzyl)-1,4,7-triaazacyclononane-1,4,7-triacetic acid (*p*-SCN-Bn-NOTA) was conjugated to the amino surface groups of the respective NPs. Efficient radiolabeling of NOTA-functionalized NPs with the positron emitter ^{64}Cu was found. The biodistribution and PET studies showed a rapid renal clearance from the *in vivo* systems for both variants of the nanoparticles. Interestingly, the different derivatives investigated exhibited significant differences in the biodistribution and pharmacokinetic properties. This can mostly be attributed to different surface charge and hydrophilicity of the NPs, arising from the synthetic strategy used to prepare the particles.

Introduction

Nowadays, nanoparticles (NPs) are considered as promising systems for the development of new medical tools.[1-9] Although NPs play an important role in current medical research, they may present toxicity and stability issues, potential unwanted accumulation in organs/tissues and lack of approved synthetic routes under the conditions of good manufacturing practice. These aspects still limit their *in vivo* applications.[10-13] Indeed, manufacturing of well-defined, non-toxic materials, featuring appropriate biodistribution and pharmacokinetic properties is a crucial endeavor for nanomedicine.[14]

Ultrasmall (size < 5 nm) renal clearable NPs may tackle some of the issues discussed above, as they display intermediate properties between those of small molecules and larger particles. Excretion from the body via renal filtration is a particularly interesting feat in this sense, as it may reduce accumulation of NPs in organs/tissues.[15-21]

Amongst the most interesting applications, *in vivo* imaging, using NPs, is the most attractive one.[22] For several years it was semiconductor quantum dots (QDs), such as CdSe, CdS and CdTe, to be mainly proposed as alternatives to organic dyes due to their resistance against photo-bleaching, as well as intense, narrow emission spectra.[23] However, due to their elemental composition, QDs are quite cytotoxic[24] and their use has been restricted to *in vitro* labeling or for image-guided surgery.[25-27] On the other hand the use of less toxic elements, such as silicon and carbon to make the particles is more promising and some of these nanoparticles have also been tested for medical applications[28-30] and bioimaging in particular.[30-40] Several *in vitro* experiments were performed to study the cellular uptake behavior[33, 41, 42] and to assess their cytotoxicity at varying dosages in different cell lines.[43, 44] On the whole, Si NPs and CQDs offer many interesting features connected to their: i) biocompatibility, biodegradability and lack of toxicity[36, 45-48]; ii) intrinsic photoluminescence that can be tuned by controlling their morphologies and surface compositions[49-53]; iii) chemical stability; iv) the possibility to functionalize their surface through stable covalent bonds.

[1]*Institute of Radiopharmaceutical Cancer Research, Helmholtz-Zentrum Dresden - Rossendorf, Bautzner Landstraße 400, Dresden, D-01328, Germany.*
[2]*Laboratoire de Chimie et des Biomatériaux Supramoléculaires, Institut de Science et d'Ingénierie Supramoléculaires (ISIS), 8 allée Gaspard Monge, Strasbourg, 67000, France.*
[3]*Institut fuer Nanotechnologie (INT), Karlsruher Institut fuer Technologie (KIT) Campus North, Hermann-von-Helmholtz-Platz 1, Eggenstein-Leopoldshafen, 76344, Germany.*
[4]*Department of Chemical Sciences, University of Padova, Via Marzolo 1, 35131 Padova, Italy.*
 # These authors contributed equally
Corresponding authors: h.stephan@hzdr.de, decola@unistra.fr
DOI: 10.1039/x0xx00000x

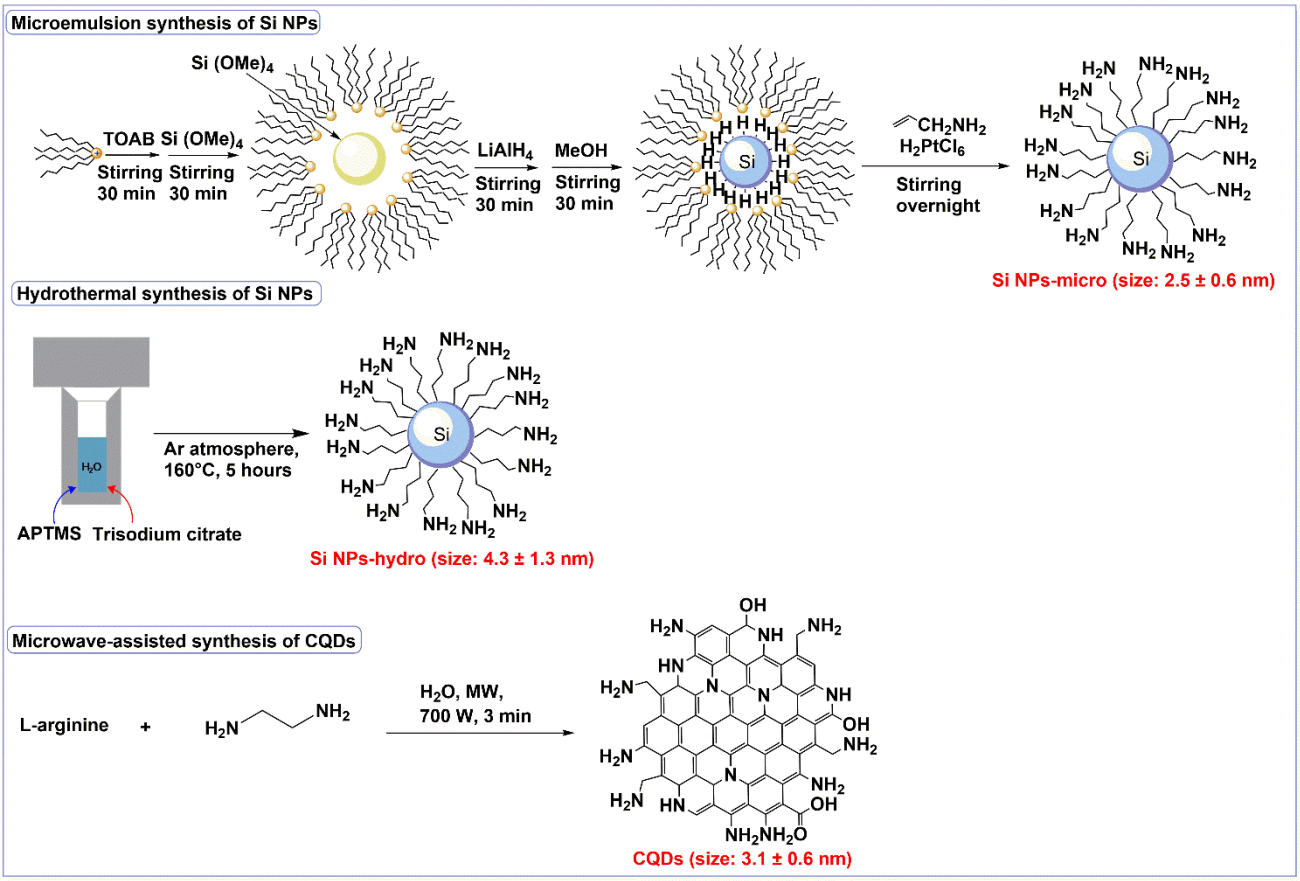

Fig. 1 Synthetic routes for the synthesis of amine-terminated Si NPs (via microemulsion-supported and hydrothermal approaches) and CQDs (via microwave-assisted synthesis).

Given the similarities between silicon and carbon, it is very appealing to study and compare the *in vivo* behavior of ultrasmall Si NPs and CQDs.[54] To date, only a few biodistribution studies of renal clearable nanoparticles incorporating radiolabels have been reported. Collectively, these studies show indeed the high potential of such NPs for *in vivo* imaging[55-60], even though no clear correlations were made with the obtained results and the different methodologies used to make the particles or the effect of the labeling units on the surface of the systems.

Herein, we tackle all these open questions and describe the preparation and characterization of ultrasmall Si NPs and CQDs. Nanotoxicity of all the NPs prepared was assessed *in vitro* upon exposure to the kidney. The labeling was achieved by functionalization of the particle surface with NOTA (1,4,7-triaazacyclononane-triacetic acid) as bifunctional chelator for radiolabeling. The NOTA-containing NPs were efficiently labeled with the positron emitter ^{64}Cu. We also investigated optical imaging by covalently linking a near-infrared dye (Kodak-X-Sight 670) on the surface of the particles. Nuclear medical imaging techniques such as PET and single-photon emission computed tomography (SPECT)[13] allows the collection of reliable information about the behavior of the NPs *in vivo*. Hence, we report biodistribution and pharmacokinetic properties of ^{64}Cu-labeled Si NPs and CQDs in healthy male Wistar rats and tumor-bearing mice.

Results and discussion

Synthesis and characterization of nanoparticles

Water-dispersible ultrasmall amine-terminated Si NPs were prepared by two different strategies: the bottom-up wet methods based on microemulsions[31] (Si NPs-micro) and the hydrothermal conditions[61] (Si NPs-hydro). CQDs were prepared by microwave-assisted treatment of an aqueous solution of L-arginine and ethylenediamine.[53] A general scheme for the preparation methods and the sizes of the three different kinds of NPs can be seen in Fig. 1.

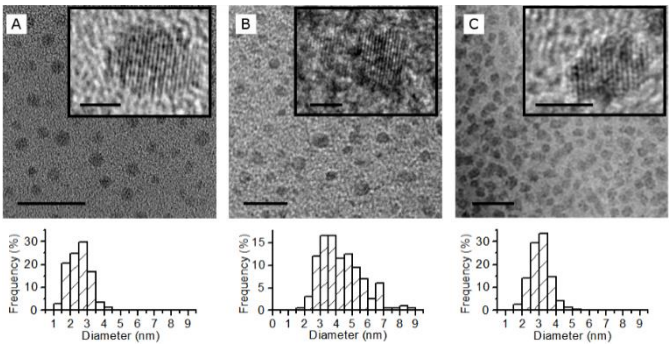

Fig. 2 HR-TEM images and size distribution graphs of Si NPs and CQDs. (A) Si NPs-micro. (B) Si NPs-hydro. (C) CQDs. Scale bars are 10 nm in the images, 2 nm in the insets.

The morphology, chemical composition and the photophysical characterizations of the Si NPs and CQDs were performed by several analytical techniques. Transmission electron microscopy (TEM) images showed monodisperse Si NPs and CQDs in the size range of 2 to 5 nm (Fig. 2). According to the distribution histograms, the average size of Si NPs-micro is 2.5 ± 0.6 nm, Si NPs-hydro 4.3 ± 1.3 nm and CQDs 3.1 ± 0.6 nm. High resolution TEM images of a single Si NPs-micro and Si NPs-hydro (Fig. 2 insets) shows a crystal lattice of silicon with a distance of 2.0 Å between fringes that is characteristic for the lattice spacing of the (220) planes of crystalline silicon. The high magnification micrograph of a single CQD indicates a crystallinity with an inter-planar distance of 2.1 Å that is consistent with the reported (100) spacing in graphene.[62]

Si NPs used for this study displayed stable photoluminescence (PL), mainly in the blue region of the electromagnetic spectrum (ESI Figs. S1A-B). The emission spectra acquired are in accordance with previous reports.[31] It is worth noting that the excitation wavelength significantly influences the position of the emission maximum. This is more evident in the case of Si NPs-micro, while for Si NPs-hydro the emission is less tunable with the excitation wavelength, probably due to the differences in the particles and their surface compositions.[49, 63] As expected, Si NPs-micro exhibit a lower surface content of oxidized species than the ones prepared by the hydrothermal method as it is indicated in the attenuated total reflectance FTIR (ATR-FTIR) spectra by the appearance of the typical peaks for silicon oxide vibration modes between 1000 and 1100 cm^{-1} only for Si NPs-hydro (ESI Figs. S2A-B). Our future research will focus on analyzing the exact elemental composition and understanding the luminescent properties of Si NPs-hydro. As found for Si NPs, the photoluminescence of CQDs (ESI Fig. S1C) is in good agreement with previous literature reports.[37] The precursors L-arginine and ethylenediamine used for the preparation of the CQDs led to surfaces covered with amino, carboxylic and hydroxyl groups, which are responsible for multi-colored luminescence.[64, 65]

In order to exploit our NPs for *in vivo* investigations, Si NPs-micro was equipped with a near-infrared fluorescent label. The tetrafluorophenyl-activated ester of Kodak-X-Sight 670, a dye showing a bright fluorescence in the near-infrared region (emission at 755 nm), was coupled to the terminal amino groups of Si NPs-micro, enabling *in vivo* fluorescence imaging. For biodistribution experiments using a radiolabel, an isothiocyanate derivative of a BFCA based on NOTA (NOTA-Bn-SCN) was reacted with the amino groups of NPs to yield stable thiourea bonds.[66, 67] NOTA readily complexes Cu^{II} under mild conditions (room temperature, physiological pH) and is thus suitable for labeling with ^{64}Cu as an ideal positron emitter, possessing an appropriate half-life of 12.7 h.[68, 69]
Functionalization of NPs (1 mg NP/mL water) with different amounts of NOTA-Bn-SCN (0.1, 0.2, 0.4 and 0.8 µmol) was carried out to study the impact of NOTA moieties on the surface charge of the materials (ESI Fig. S3). Due to the protonated amines under physiological conditions, the overall surface charge of Si NPs-micro and CQDs is positive. The decrease in charge with an increasing NOTA coverage (zeta potential, ζ from +9.1 ± 5.5 mV to -6.3 ± 4.9 mV for Si NPs-micro and from +33.8 ± 6.3 mV to 17.7 ± 5.5 mV for CQDs), indicates the presence of the carboxylate groups that charge compensate the terminal cationic amines. Interestingly, for Si NPs-hydro, no major deflection in the zeta potential was observed (ζ in the range of -1.1 ± 3.9 mV to -2.9 ± 4.7 mV) with the increasing amount of NOTA. This finding can be explained by the formation of a stable citrate shell on the surface of the particles confirmed by NMR and IR experiments (ESI Figs. S4-S7). ^{1}H NMR experiments using a D_2O solution of the NPs revealed an upfield shift of the proton signals (δ = 2.67 and 2.54 pm to δ = 2.40 and 2.27 pm). Furthermore, integration of the signals and comparison with the signals assigned to the NPs showed a 1/6 ratio of the citrate compared to the *n*-propylamine residue.

Table 1 Distribution ratio log $D_{7.4}$ of ^{64}Cu-labeled NPs as function of NOTA content.

NOTA [µmol/mg NPs]	NOTA-Si NPs-hydro	NOTA-Si NPs micro	NOTA-CQDs
0.1	-4.12 ± 0.04	-2.56 ± 0.01	-1.71 ± 0.01
0.2	-	-2.36 ± 0.02	-
0.4	-3.71 ± 0.11	-2.05 ± 0.01	-1.63 ± 0.01
0.8	-3.14 ± 0.02	-2.09 ± 0.01	-1.94 ± 0.01
log $D_{7.4}$ ([^{64}Cu]Cu-NOTA-Bn-NH_2: -4.16 ± 0.10); log $D_{7.4}$ ([^{64}Cu]Cu-NOTA-Bn-SCN: -2.13 ± 0.01)			

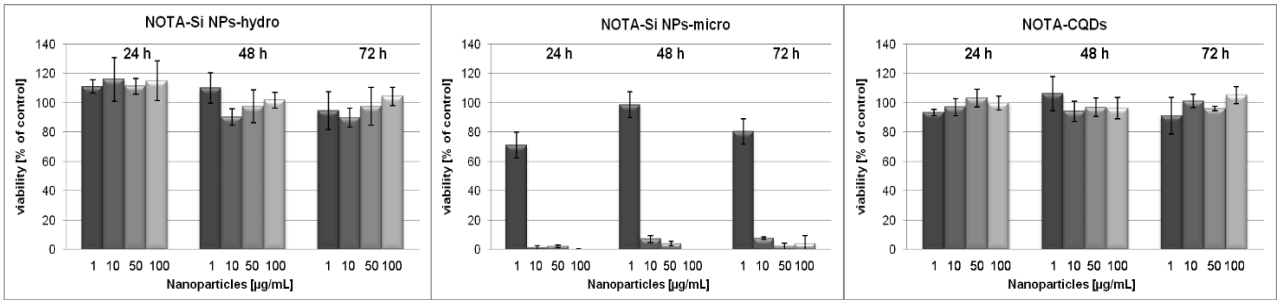

Fig. 3 Effect of NOTA-Si NPs-hydro (left), NOTA-Si NPs-micro (center) and NOTA-CQDs (right) on the viability of HEK293 cells. The cells were exposed to 1, 20, 50 and 100 µg/mL nanoparticle dispersions for 24, 48 and 78 h respectively in Dulbecco's modified eagle's medium (DMEM) supplemented with 10 % fetal bovine serum (FBS) and viability was determined using a standard MTS assay.

Assuming if each cationic amine is getting neutralized by one of the three carboxylates of the citrate, then half of the surface amine groups of the NP will be neutralized. The pattern of the NPs ^{13}C NMR spectrum supports this finding as well as the zeta potential results. To prove the influence of temperature on the binding of citrate to the NPs, temperature-dependent ^{1}H NMR spectroscopy (range: 10-45°C) were performed, but no significant difference in the ratio or the chemical shift of the signals was observed.

Radiolabeling of nanoparticles

NOTA-functionalized NPs were labeled with [^{64}Cu]$CuCl_2$ in MES/NaOH buffer (pH 6) at room temperature for 30 min. Radio-iTLC (radio instant thin layer chromatography) confirmed full complexation and no trace of free $^{64}Cu^{II}$ (ESI Fig. S8). The stability of the ^{64}Cu-labeled nanoparticles was tested in challenge experiments using 10,000-fold excess of EDTA and 1,000-fold excess of 1,4,8,11-tetraazacyclotetradecane-1,4,8,11-tetraacetic acid (TETA) at 38°C for 24 h with no indication of transchelation. The results are in accordance with former investigations[67, 70-72] and confirm NOTA as an appropriate chelating agent for ^{64}Cu-labeling of nanoparticles. The distribution behavior of the ^{64}Cu-labeled NPs was determined in a two-phase 1-octanol/aqueous buffer system. The log $D_{7.4}$ value (distribution ratio at pH 7.4) is an important indicator for the prediction and interpretation of the distribution properties of compounds in living systems.[73] As summarized in Table 1, these NPs are quite hydrophilic in character with distribution ratios log $D_{7.4}$ in the range of -4.2 to -1.6 which is typical for renal clearable compounds. The log $D_{7.4}$ value of ^{64}Cu-labeled CQDs was not significantly influenced by varying the amount of NOTA. In contrast, an increasing NOTA content on the surface of Si NPs led to a gradual decrease in its hydrophilicity.

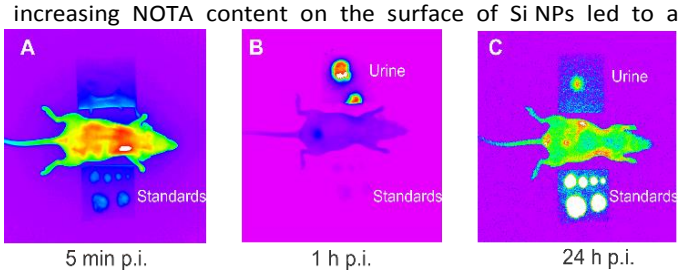

Fig. 4 *In vivo* fluorescence images of NMRI nu/nu mouse post injection of Kodak-XS-670-labeled Si-NPs-micro.

Nanotoxicity of Si NPs and CQDs

To assess the toxicity of these nanoparticles, the viability of human embryonic kidney cells (HEK293) was tested in the presence of NOTA-modified and amine terminated NPs using an MTS (3-(4,5-dimethylthiazol-2-yl)-5-(3-carboxymethoxy-phenyl)-2-(4-sulfophenyl)-2*H*-tetrazolium) assay. A kidney cell line was chosen because the preferred excretion pathway for this kind of NPs is renal. Fig. 3 shows the results of the performed experiments after incubation of Si NPs and CQDs (0.1 µmol NOTA/mg NPs) for 24, 48 and 72 h. The metabolic activity of the cells was not substantially influenced upon exposure to 1-100 µg/mL NOTA-Si NPs-hydro and NOTA-CQDs for up to 72 h. This is in accordance to literature data. Indeed, the reported MTT assays for CQDs showed a high viability of cells after NPs exposure to HepG2 human hepatocellular carcinoma cells and MG 63 cells[34, 74] and literature on amine-terminated Si NPs prepared by the hydrothermal method revealed very low cytotoxicity in human epithelial cervical cancer cells (HeLa) even after 48 h of exposure.[61] Similar cytotoxicity results have been reported for amine-terminated Si NPs (size: 4.5 nm) prepared by galvanostatic anodization of porous silicon layer and exposed to HepG2 (human liver hepatocellular carcinoma)[75] to Caco-2 (human colorectal adenocarcinoma) and CCD-841 (human normal colon epithelial) cells.[76] In contrast, Si NPs-micro slashed the viability of cells upon exposure to even low NPs concentrations ≥ 10 µg/mL. This can be attributed to both the presence of residual traces of surfactant (tetraoctylammonium bromide) coming from the NPs synthesis and the high density of terminal amino groups indicated by a positive zeta potential (ζ = +5.57 ± 4.62 mV). It is well-known that amino-containing polymers such as polyethylene imine and dendrimers are quite cytotoxic.[77] The same is true for ultrasmall amine-terminated Si NPs as previously reported.[43, 44, 78] Viability studies in human colonic adenocarcinoma Caco-2 and rat alveolar macrophage NR8383 cell lines revealed that NH_2-containing Si NPs are cytotoxic whilst their neutral or COOH-terminated analogues are non-cytotoxic. In addition, it was shown that the toxicity of amine-terminated Si NPs increases in the presence of serum[43] and this was ascribed to the fact that serum proteins facilitate the cellular uptake of NPs and thus cause higher toxicity.[79, 80]

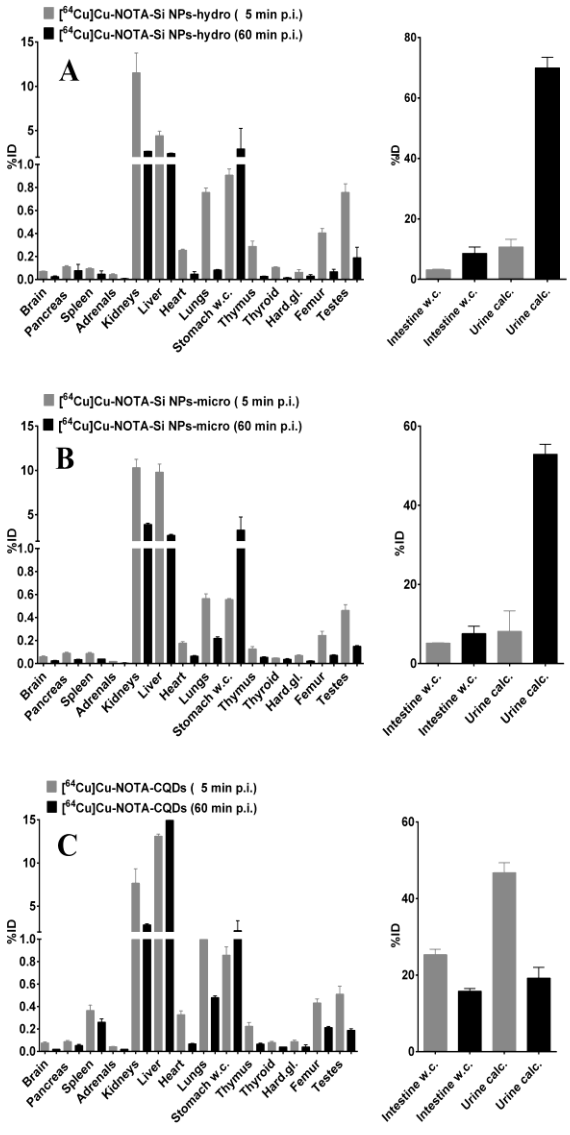

Fig. 5 Biodistribution of [^{64}Cu]Cu-NOTA-Si NPs-hydro (**A**), [^{64}Cu]Cu-NOTA-Si NPs-micro (**B**) and [^{64}Cu]Cu-NOTA-CQDs (**C**) in male Wistar rats at 5 and 60 min after single intravenous application (w.c. = with content). Data expressed as % ID (mean ± SD of 4 animals).

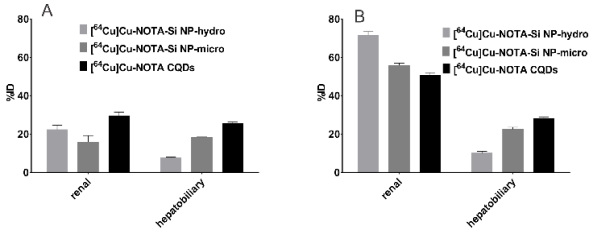

Fig. 6 Elimination of [^{64}Cu]Cu-NOTA-Si NPs-hydro, [^{64}Cu]Cu-NOTA-Si NPs-micro and [^{64}Cu]Cu-NOTA-CQDs. Total body clearance of nanoparticles 5 min (**A**) and 60 min (**B**) after single intravenous injection into rats (mean ± SD, 4 animals). All values are significant different in comparison to the others.

The same cytotoxicity assay was performed with NPs before functionalization with NOTA and it does not show significant differences, indicating that the surface modification with the chelator does not influence particularly the cell viability.

Fluorescence imaging of Kodak-XS-670-labeled Si NPs-micro

In a first experiment, fluorescent-labeled Si NPs-micro were administered to a NMRI nu/nu mouse and biodistribution was assayed with an *in vivo* fluorescence imaging system Kodak FX. The images at 5 min, 60 min and 24 h showed that the Kodak-XS-670-labeled Si NPs-micro were rapidly eliminated through the kidneys into the bladder (Fig. 4), whereby the particles were temporarily retained in body regions of the lymphatic system. This was confirmed by *ex vivo* fluorescence measurements of 80 µm whole-body frozen sections, indicating little subcutaneous accumulation at 60 min (ESI Fig. S10). Importantly after 24 h no fluorescence originating from the particles was detected in the body with exception of traces in the bladder.

Biodistribution of ^{64}Cu-labeled Si NPs and CQDs in male Wistar rats

Biodistribution of ^{64}Cu-labeled NOTA-containing Si NPs and CQDs was studied in male Wistar rats by organ and tissue extraction. The data are compiled for the accumulated activity amount (% ID = % injected dose, Fig. 5 and ESI Table S1) and the resulting activity concentration (SUV = activity concentration in the tissue/injected activity x body weight, ESI Table S2). As can be seen from Fig. 4, the particles were rapidly excreted from the body, showing only a small but significant difference in the clearance profile (Fig. 6). The nearly neutral (ζ = -1.1 ± 3.9 mV) and most hydrophilic Si NPs-hydro were eliminated most rapidly from the body, predominantly via the renal pathway into urine (> 70 % of ID, 60 min p.i.). It is worth to mention that only a very small amount of [^{64}Cu]Cu-NOTA-Si NPs-hydro was found in the liver (1.4 ± 0.04 % ID, 60 min p.i.). In contrast, the ^{64}Cu-labeled positively charged particles NOTA-Si NPs-micro (ζ = +5.57 ± 4.62 mV) and NOTA-CQDs (ζ = +33.8 ± 6.3 mV) with lower hydrophilicity showed significant accumulation in liver and intestine ([^{64}Cu]Cu-NOTA-Si NPs-micro: 2.67 ± 0.07 % ID in liver, 25.32 ± 1.42 % ID in intestine; [^{64}Cu]Cu-NOTA-CQDs: 14.93 ± 0.21 % ID in liver, 7.58 ± 1.86 % ID in intestine; 60 min p.i.). The different biodistribution behavior may be attributed to the formation of a protein corona. Charged nanoparticles are prone to adsorb proteins on their surfaces[10, 81], leading to an increased uptake particularly in the liver while almost zero protein adsorption was observed for neutral and zwitterionic nanoparticles.[82-84] Collectively, all the three kinds of particles investigated here are rapidly cleared from the blood in an hour, accounting about 80 % of the injected activity. However, [^{64}Cu]Cu-NOTA-Si NPs-hydro showed the most promising biodistribution profile with rapid renal excretion into the urinary bladder. A comparable fast excretion was found for ^{64}Cu-labeled CuS nanodots stabilized with polyvinylpyrrolidone (PVP).[59] These PVP-coated CuS nanodots were even more rapidly excreted from the body than the very small (< 5 nm) tiopronin- and glutathione-coated gold nanoparticles as well as PEGylated

Cu-Au alloy nanoclusters.[55, 57, 85] Very recently, it was shown that ultrasmall (3 nm) Cu-based nanoclusters and gold clusters (4.5 nm) equipped with tumor-specific peptides were predominantly renally excreted and considerably accumulated in tumors.[58, 60]

NOTA-Si NPs-micro), and 9.9 min ([^{64}Cu]Cu-NOTA-CQDs) were calculated (ESI Table S4). The activity plateaus of the NPs in the urine and bladder were different showing the maximum for [^{64}Cu]Cu-NOTA-Si NPs-hydro (84.5 % ID), followed by [^{64}Cu]Cu-NOTA-Si NPs-micro (67.4 % ID), and the lowest for the

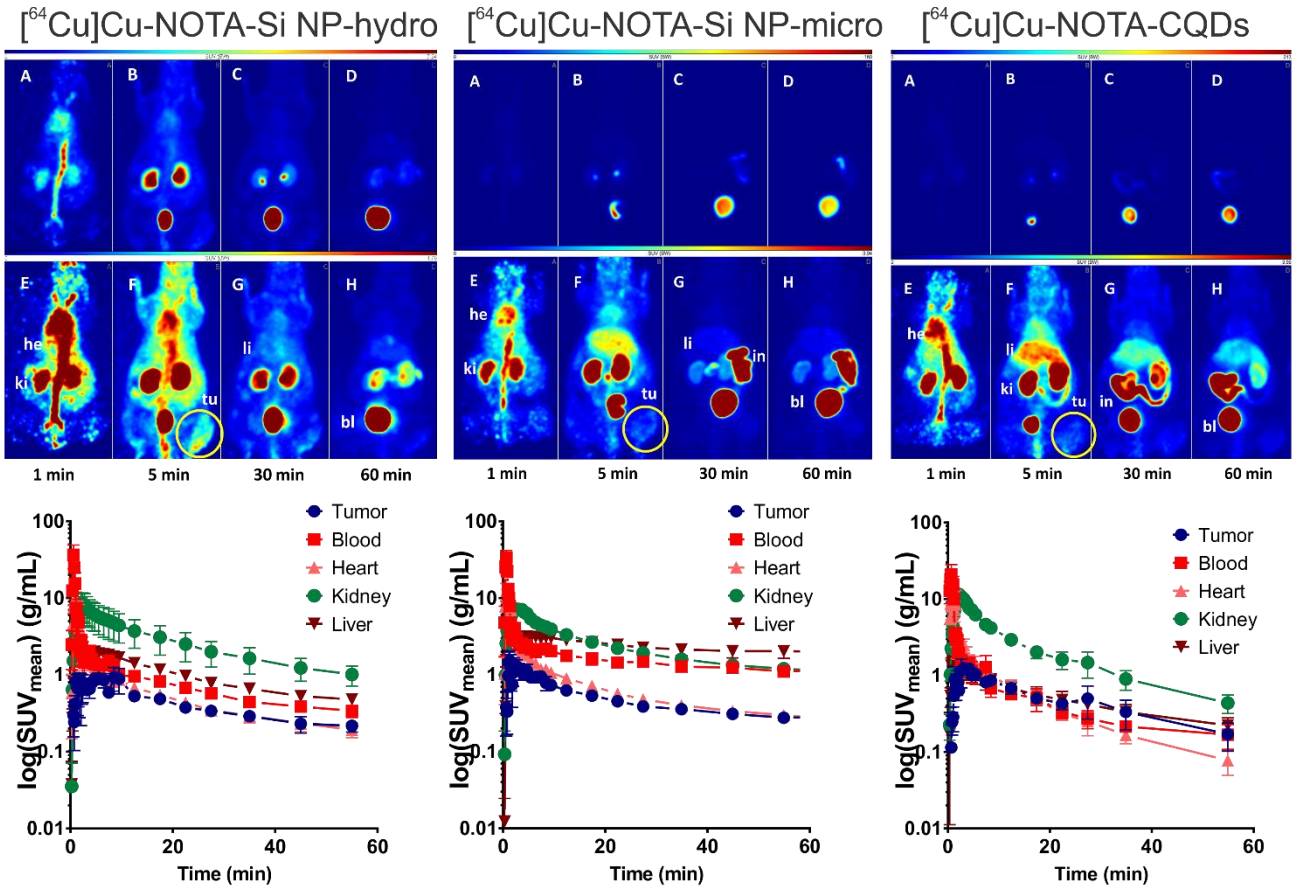

Fig. 7 Maximum intensity projections obtained from a PET study after a single intravenous injection of [^{64}Cu]Cu-NOTA-Si NPs-hydro (n = 2), [^{64}Cu]Cu-NOTA-Si NPs-micro (n = 2) and [^{64}Cu]Cu-NOTA-CQDs (n = 4) in a A431 tumor-bearing mice after 1 min (A, E), 5 min (B, F), 30 min (C, G), and 60 min (D, H) after injection. The images A-D were scaled to the maximum activity and the images E-H were rescaled to visualize the tumor (Above). Time activity curves of the activity concentration (log SUV) (Below). Abbreviations: bl= bladder, he= heart, in= intestine, ki= kidney, li= liver, tu= tumor. Values are presented as mean ± SEM.

Small animal PET of ^{64}Cu-labeled Si NPs and CQDs in murine A431 tumor xenograft NMRI nu/nu mice

The biodistribution profile of ^{64}Cu-labeled nanoparticles was also evaluated by dynamic PET experiments in female NMRI nu/nu mice, bearing epidermoid carcinoma (A431) xenografts on the right hind leg (Fig. 7). PET/CT images are presented in Supplementary Information (ESI Fig S9) to show both localization of the activity concentration in the body and appropriate anatomical information. As expected, the results obtained are very similar to the biodistribution data observed with Wistar rats. The particles were rapidly cleared from the body (Fig. 8). The blood clearance profile was similar for both the types of Si NPs with half-lives of 8.2 min ([^{64}Cu]Cu-NOTA-Si NPs-hydro) and 10.5 min ([^{64}Cu]Cu-NOTA-Si NPs-micro). [^{64}Cu]Cu-NOTA-CQDs were cleared from blood rather slowly ($t_{1/2}$: 11.4 min). The renal elimination into urine followed a one-phase association model. Based on this model, half-lives of 9.3 min ([^{64}Cu]Cu-NOTA-Si NPs-hydro), 8.6 min ([^{64}Cu]Cu-

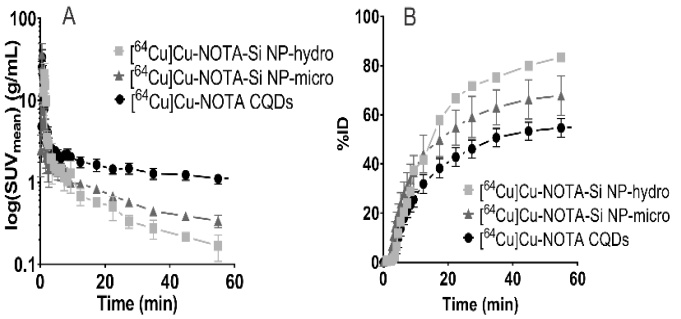

Fig. 8 (**A**) Blood activity concentration time curves of [^{64}Cu]Cu-NOTA-Si NPs-hydro (n=2), [^{64}Cu]Cu-NOTA-Si NPs-micro (n=2), and [^{64}Cu]Cu-NOTA-CQDs (n=4) in A431 tumor bearing mice (see Table S3). Values are mean ± SEM. (**B**) Bladder plus urine activity amount time curves of [^{64}Cu]Cu-NOTA-SI NPs-hydro (n=2), [^{64}Cu]Cu-NOTA-SI NPs-micro (n=2), and [^{64}Cu]Cu-NOTA-CQDs (n=4) in A431 tumor-bearing mice. Values are mean ± SEM (ESI Table S4).

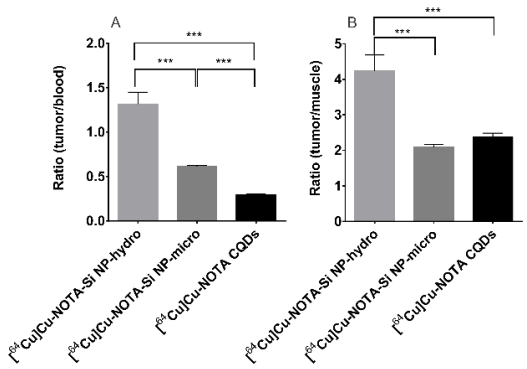

Fig. 9 Tumor to blood (**A**) and tumor to muscle (**B**) ratios of [^{64}Cu]Cu-NOTA-Si NPs-hydro (n=2), [^{64}Cu]Cu-NOTA-Si NPs-micro (n=2), and [^{64}Cu]Cu-NOTA-CQDs (n=4) in a A431 tumor-bearing mice after single intravenous injections. Values were calculated from the time activity curves (ESI Fig. S11) as ratio mean ± SEM between 15 and 60 min after injections.

[^{64}Cu]Cu-NOTA-CQDs (55.9 % ID).

As shown in Fig. 7, the radiolabeled particles were rapidly distributed in the tumor which allows a clear visualization particularly at the early time points (5 min i.v.). In this respect, [^{64}Cu]Cu-NOTA-Si NPs-hydro showed the most favorable properties with the highest tumor-to-blood-(muscle) ratio (Fig. 9). However, the activity was quickly washed out from the tumor in case of all the investigated particles as expected for small sized particles[19], with the exception of NPs equipped with tumor-specific peptides which can reside longer in the tumor.[58, 60] Altogether, Si NPs-hydro showed the most promising features for further modification in view of tumor imaging and treatment.

Conclusions

In summary, a comparative biodistribution study of ultrasmall silicon nanoparticles and carbon dots (size below 5 nm) was performed. In this regard, the particles were equipped with a NOTA tag for labeling with ^{64}Cu as a positron emitter, allowing the acquisition of reliable information of biodistribution using PET. Small animal studies with Wistar rats and tumor-bearing mice showed that all the particles were rapidly excreted from the body. The behaviour of the particles described, both *in vitro* and *in vivo*, was mainly dictated by their surface features. Their toxicity was correlated to the extent of amine group surface coverage, as well as the traces of surfactant remaining after their synthesis and purification. Moreover, we found that the surface charge of the nanomaterials, characterized by their zeta potential value, plays a major role in their biodistribution. In particular, particles with positive zeta potentials showed significant accumulation in liver and intestine. This is probably due to the formation of a protein corona, contrary to neutral/zwitterionic particles that were the fastest to be cleared via the renal pathway with very little liver uptake. The citrate-stabilized particles showed the most promising biodistribution profile. Nevertheless, Si NPs-micro and CQDs also represent promising platforms for future applications as nanoscale imaging agents, particularly when a neutral surface charge is achieved. The easily accessible functional groups on the nanoparticle surface allows the facile synthesis of dual-labeled (dye and radiolabel) ultrasmall materials equipped with small active targeting agents such as peptides for tumor imaging. Fluorescence and nuclear imaging will provide useful information for a systemic evaluation of biodistribution and pharmacokinetic properties required for biomedical applications.

Experimental Section

All chemicals were purchased from commercial suppliers and used as received without further purification. *S*-2-(4-Isothiocyanatobenzyl)-1,4,7-triazacyclononane-1,4,7-triacetic acid (SCN-Bn-NOTA; #B-605) was purchased from Macrocyclics. Toluene (extra dry over molecular sieve 99.85%) was deaerated by constant bubbling of argon inside the bottle for 20-30 minutes. Methanol was deaerated likewise. Allylamine was dried over $CaCl_2$ overnight, distilled and deaerated before use. A Direct-Q 3 UV water purification system from Millipore (Merck KGaA) was applied for producing deionized water. The resistance of deionized water was 18.2 MΩ•cm. Dialysis tubes were purchased from Serva (MWCO: 1 kDa; Spectra/Por® 7 dialysis tubing). High pressure resistant home-made Teflon vessels (similar to those reported by Calzaferri et al.[86]) were used for hydrothermal syntheses throughout this work.

Particle characterization techniques

NMR experiments were accomplished using a 600 MHz Agilent DD-2 spectrometer with OneNMR probe (5 mm, ^{1}H: 600 MHz, ^{13}C: 151 MHz). Samples for NMR were prepared using a lower glass stem tube filled with deuterated water as external lock/reference material and a small quantity of NPs in a minimum quantity the water volume (in the case of the NPs solution). Water suppression was done using the PreSat experiment with D_2O/H_2O as standard and ^{1}H/^{13}C-HSQC was done using the HSQCAD experiment of the OpenVnmrJ program package.

Samples for HR-TEM were prepared by drop-casting an ethanol solution of the sample on carbon-coated copper grids (Quantifoil, GmbH). The analysis was performed using a FEI Titan 80-300 transmission electron microscope operated at 300 KV. Size distribution histograms were built counting 200 nanoparticles.

Absorption spectra were acquired using a double-beam Shimadzu UV-3600 UV-Vis-NIR spectrophotometer. Steady-state emission spectra were recorded on a HORIBA Jobin-Yvon IBH FL-322 Fluorolog 3 spectrometer equipped with a 450 W xenon arc lamp, as the excitation source, and a TBX-4-X single-photon-counting device as the detector. Emission spectra were corrected for source intensity (lamp and grating) and emission spectral response (detector and grating) by standard correction curves. PLQY were measured on a Hamamatsu Quantaurus-QY integrating sphere equipped with a 150 W CW Xenon source.

FT-IR spectra were acquired on a Shimadzu IR Affinity-1 spectrometer used in attenuated total reflectance (ATR) mode.

Zeta potential measurements were performed on a Zetasizer Nano ZS (Malvern Instruments GmbH, Germany) in DTS 1060 capillary cells at 25°C. Samples were prepared in deionized water (pH 6.8), 10 mM NaCl-solution (pH 6.6) or phosphate-buffer (10 mM, pH 6.8) with a concentration of 0.3 mg/ml. The given values of zeta potential comprise the average value from three unbiased set of data of 100 measurements each. According to literature data for water, a viscosity of $\mu = 0.8872$ cP and a dielectric constant of $\varepsilon = 78.5$ was used. Analysis of data was performed utilizing Zetasizer Software 6.12 (Malvern Instruments GmbH, Germany) based on the model of Smoluchowski.

Synthesis of silicon nanoparticles by microemulsion method (Si NPs-micro)

Silicon nanoparticles Si NPs-micro were prepared using a slight modification of a reported method. [31] The reaction was performed in a nitrogen glove box (H_2O and O_2 levels < 0.1 ppm). 7.5 g of tetraoctylammonium bromide was mixed with 100 mL of dry toluene and the mixture was stirred for 30 min. Then, 0.5 mL of $Si(OCH_3)_4$ was added and stirring was continued for 30 min allowing the silicon precursor to enter the micelles. Subsequently, 7 mL of $LiAlH_4$ (1 M in THF) was added to reduce the silicon precursor and to form hydrogen-terminated Si NPs. After 30 min of stirring, dried and deaerated methanol (3.2 mL) was added to quench the excess of $LiAlH_4$. The quantity of MeOH was minimized in respect to previous reported methods to avoid the formation of methoxy-terminated Si NPs. The final amine-terminated NPs were obtained by adding distilled and degassed allylamine (13 mL) in the presence of 0.2 mL of H_2PtCl_6 catalyst (0.05 M in MeOH). After stirring overnight, Si NPs modified with 3-aminopropyl groups were extracted with water, washed with ethyl acetate and filtered twice using syringe membrane filters (Millex, Millipore, PVDF, 0.45 µm). The resulting Si NPs were purified by size exclusion chromatography (Sephadex LH-20) with MeOH as eluent.

Synthesis of silicon nanoparticles using hydrothermal method (Si NPs-hydro)

Amine-terminated nanoparticles were prepared by modifying a reported method.[61] 0.82 g of trisodium citrate was added to 20 mL of argon-saturated Milli-Q water. After stirring and bubbling with argon for 15 minutes, 5.0 mL of aminopropyltrimethoxysilane (APTMS) was added to the aqueous citrate solution and stirred under Ar for 15 minutes. This mixture was then transferred into a Teflon vessel while constantly bubbling Ar. The precursor solution was heated at 160 °C for 5 h in a conventional oven. After cooling down to room temperature, the sample was purified by dialysis (dialysis tube: MWCO: 1 kDa) against water.

Synthesis of carbon quantum dots (CQDs)

CQDs were prepared according to a reported method[53] by microwave treatment of an aqueous solution of L-arginine hydrochloride (2 M) and ethylenediamine (2 M). 5.6 g of L-arginine hydrochloride and 1.78 mL of ethylenediamine were dissolved in 13.3 mL of deionized water. The solution was placed in a common domestic microwave oven for 3 minutes at a nominal power of 700 W under normal pressure. After the reaction, CQDs were purified by dialysis against water (MWCO = 1 kDa). 1.2 g CQDs were produced using this protocol.

Conjugation of Kodak X-Sight-670 fluorescent dye to Si NPs-micro

36 µL amino-terminated silicon nanoparticles Si NPs-micro dispersed in water (c = 2 mg/mL) were added to 964 µL phosphate buffer (10 mM, pH 7.5). Then, 1 mg (0.88 µmol) Kodak X-Sight-670 tetrafluorophenyl ester (Carestream Health, USA) was added and the mixture was stirred for 3 h at room temperature. Unreacted material was separated by dialysis (MWCO: 7 kDa, Serva, Membra-Cel) until the solvent becomes colorless (8 times with 300 mL H_2O each in 8 h cycles).

Coupling of SCN-Bn-NOTA to Si NPs and CQDs

NOTA-Si NPs-micro, NOTA-Si NPs-hydro and NOTA-CQDs were prepared dispersing 1 mg of amine-terminated Si NPs (either prepared by microemulsion or by hydrothermal method) or CQDs in 150 µL of deionized water and placed in a 1.5 mL low protein binding Eppendorf-tube. A specific amount of SCN-Bn-NOTA (0.1, 0.2, 0.4 and 0.8 µmol per mg of nanoparticles) was dissolved in 100 µL of deionized water and was added to the dispersion of NPs. The final dispersion was then shaken on a thermo-mixer (Eppendorf) at 750 rpm for 16 h at 25°C. All samples prepared for *in vivo* experiments were purified by dialysis against deionized water (MWCO 0.5 – 1 kDa, Spectra Por Float-A-Lyzer G2, 1 mL). Afterwards a defined aliquot was freeze-dried to obtain the final concentration of particles.

***In vitro* assessment of of nanotoxicity**

All cell culture reagents were purchased from Biochrom AG and Sigma-Aldrich unless otherwise specified. Cell culture flasks, dishes and plates were supplied by Greiner Bio-One GmbH. The human embryonic kidney cell line HEK293 (DSMZ no.: ACC 305) was cultured as previously reported.[84, 87, 88] The cell line was confirmed to be mycoplasma-negative and was tested monthly. To assess cell viability following nanoparticle exposure, HEK293 cells were seeded in 96-well cell culture plates (~ 5000 cells/0.1 mL/well) and were grown for 24 h. The cell viability was measured using the CellTiter 96® AQueous One Solution Cell Proliferation Assay (MTS, Promega Corporation) according to the manufacturer's instructions. With this colorimetric assay, the activity of cellular enzymes is determined, since these proteins reduce the tetrazolium compound 3-(4,5-dimethylthiazol-2-yl)-5-(3-carboxymethoxy-phenyl)-2-(4-sulfophenyl)-2*H*-tetrazolium (MTS) to purple-colored formazan, which can be quantified by recording the absorbance at 490 nm.

Radiolabeling experiments

The production of ^{64}Cu was performed at a Cyclone® 18/9 (Helmholtz-Zentrum Dresden-Rossendorf). For the $^{64}Ni(p,n)^{64}Cu$ nuclear reaction, 15 MeV protons with a beam current of 12 µA for 150 min were used. The yields of the

nuclear reaction $^{64}Ni(p,n)^{64}Cu$ were 3.6-5.2 GBq [at the end of bombardment (EOB)] with molar activities of 150–250 GBq μmol^{-1} Cu diluted in HCl (10 mM).[89] An aliquot of [^{64}Cu]$CuCl_2$ solution (20–100 MBq) was buffered with MES (2-(*N*-morpholino)ethanesulfonic acid)/NaOH-buffer (0.1 M; pH 6). Typically, a specific amount of nanoparticles, up to 10 μg, was mixed in a 1.5 mL low protein binding Eppendorf-tube with a specific aliquot of [^{64}Cu]$CuCl_2$-solution (varying up to 40 MBq) and addition of MES/NaOH buffer (0.1 M; pH 6) up to a final volume in the range of 150-200 μL. The particles were labeled by means of mechanical shaking for 30 min at 25 °C. The specific activity of the nanoparticles (0.1 μmol NOTA/mg NP) was ~ 4 GBq/mg NPs. To check the full labeling, 2 nmol EDTA was added to a 5 μL aliquot of the solution and the labeling process of the nanoparticles (R_f = 0) was monitored by radio-TLC on iTLC-SA plates (instant TLC medium impregnated with salicylic acid, Agilent Technology) using 0.9% NaCl in H_2O as mobile phase. As control, separate radio-TLC analysis of [^{64}Cu]Cu–EDTA (R_f = 0.9) was performed in the same mobile phase. Evaluation of radio-TLC was carried out using a radioactivity thin layer analyzer (Rita Star, Raytest**,** Germany). ^{64}Cu-labeled nanoparticles were challenged with a 10.000-fold excess of EDTA and a 1.000-fold TETA (24 h, at 38°C). Radio-iTLC analysis (see above) was used to monitor the stability of ^{64}Cu-labeled NPs (^{64}Cu-NPs, R_f = 0; [^{64}Cu]Cu-EDTA and [^{64}Cu]Cu-TETA, R_f = 0.9). 1-octanol-water distribution coefficients were determined for the ^{64}Cu-labeled nanoparticles. Aliquots of radiolabeled nanoparticles (50 μL with a concentration of 1 μg NPs/mL) were added to 450 μL of 0.05 M of HEPES-NaOH buffer at pH 7.4 and then 0.5 mL 1-octanol was added. The distribution experiments were carried out at room temperature in microcentrifuge tubes (2 cm^3) with mechanical shaking for 30 min. All samples were centrifuged and the phases then separated. The copper concentration in both phases was determined radiometrically using a γ–radiation gamma counter 1480, Wizard 3, Perkin Elmer. The results are average values of one experiment with repeat determination.

Animal experiments

Animal experiments were carried out according to the guidelines of the German Regulations for Animal Welfare. The local Ethical Committee for Animal Experiments approved the animal facilities and the protocol according to institutional guidelines and the German animal welfare regulations (reference numbers 24D-9168.11-4/2007-2 and 24-9168.21-4/2004-1). Male Wistar rats (Harlan Winkelmann GmbH, Borchen, Germany) between 7 and 9 weeks of age and female NMRI nu/nu mice (aged 7-14 weeks; Technische Universität Dresden, Oncoray, Germany) were housed in an Animal Biosafety Level 1 (ABSL-1) acclimatized facility with a temperature of 22 ± 2°C and humidity of 55 ± 5%. For PET experiments in tumor-bearing mice, about 2x10^6 A431 cells (ATCC number: CRL-1555) were injected subcutaneously in the back or right hind leg of NMRI nu/nu mice according to the protocol published elsewhere.[90]

Animals were kept under a 12 h light cycle in temperature-controlled airflow cabinets (27 ± 1°C) and had free access to standard pellet feed and water.

Fluorescence imaging

An aqueous solution (870 μg Kodak-XS-670-Si NPs-micro/mL) was used for *in vivo* fluorescence imaging. In a typical experiment, 200 μL of this solution was administered to a NMRI nu/nu mouse. *In vivo* fluorescence images of NMRI nu/nu mouse using Kodak-XS-670-labeled silicon nanoparticles were exposed with a Kodak *in vivo* imaging system FX after 5 minutes, 1 and 24 h. In parallel, *ex vivo* studies on frozen sections (80 μm thickness) of NMRI nu/nu mouse were performed with mice sacrificed after (5 min, 1 h, 24 h) using a cryomicrotom (Jung Cryopolycat, Leica, Germany). The frozen sections were placed in a Kodak *in vivo* imaging system FX for fluorescence detection, and the images were analyzed using Kodak Molecular Imaging Software.

***In vivo* biodistribution**

Two groups of four rats each (5 and 60 min) were intravenously injected into a lateral tail vein with 0.5–5.0 MBq of ^{64}Cu-labeled nanoparticles, which were dissolved in 0.5 mL of electrolyte solution E-153 (Serumwerk Bernburg, Germany) at pH 7.2. The molar activity ranged from 5.0 to 30 GBq/μmol at the time of injection. Animals were sacrificed at 5 and 60 min post injection. Blood and major organs were collected, weighed, and counted in a Wallac WIZARD automatic γ-counter (PerkinElmer, Germany). The activity of the tissue samples was decay-corrected and calibrated by comparing the counts in tissue with the counts in aliquots of the injected particles that were measured in the γ-counter at the same time. The activity amount in the selected tissues and organs was expressed as percent of injected dose (% ID). The activity concentration in the biodistribution measurements were calculated as SUV [SUV = (activity/g tissue)/(injected activity/body weight)] and expressed as means ± standard deviation (mean ± SD) for each group of four animals.

***In vivo* small animal positron emission tomography (PET)**

The procedures are described in detail elsewhere.[91] Rats or mice were anesthetized (desflurane in oxygen/air (30%), positioned and immobilized prone with their medial axis parallel to the axial axis of the scanners (NanoScan PET/CT, Mediso, microPET® P4, Siemens preclinical solutions). The radiotracer was administered intravenously as an infusion using a syringe pump over one minute (Harvard Apparatus, flow rate: injection volume as mL/min) through a needle catheter into a lateral tail vein. The standardized uptake values (SUV) were calculated from the ROI as the ratio of activity concentration (Bq/mL) at time t and injected dose (Bq) at the time of injection (t_0) divided by body weight (g). For the demonstration of the increasing activity uptake, the early (mid-frame time 3 min post injection) images were subtracted from the late image (mid-frame time 50 min post injection).

Statistics

Statistical analyses were carried out with GraphPad Prism version 6 (GraphPad Software, San Diego/California, USA). The data are expressed as mean ± SEM, and were submitted to one-way analysis of variance (ANOVA) followed by Bonferroni correction. Values of $p < 0.05$ were considered statistically significant and indicated by an asterisk (*).

Conflicts of interest

There are no conflicts to declare.

Acknowledgements

We thank Utta Herzog for the excellent technical support during the cell culture work. We thank Dr. Eko Adi Prasetyanto for the valuable discussions. This work was supported by the Helmholtz Initiative and Networking Fund (Functional nanomaterials for multimodality cancer imaging (NanoTracking), project ID: VH-VI-421).

Notes

Keywords: silicon nanoparticles, carbon quantum dots, copper-64, biodistribution, small animal positron emission tomography

All additional experimental data are presented in the Supporting information section. It is available free of charge via the Internet.

Author Contributions

N.L., A.F., J.L.Z.D synthesized, purified and characterized the Si NPs. S.S. and M.M. synthesised, purified and characterized the CQDs. C.M. performed the NMR experiments. S.H. and G.S. performed the radiolabeling experiments and *in vitro* characterization. R.B. and S.H. designed and performed the *in vivo* study and data analysis. L.D.C. and H.S. conceived the study. N.L., S.H., L.D.C and H.S. wrote the paper with input from all authors.

References

1. B. Pelaz, S. Jaber, D. J. de Aberasturi, V. Wulf, T. Aida, J. M. de la Fuente, J. Feldmann, H. E. Gaub, L. Josephson, C. R. Kagan, N. A. Kotov, L. M. Liz-Marzán, H. Mattoussi, P. Mulvaney, C. B. Murray, A. L. Rogach, P. S. Weiss, I. Willner and W. J. Parak, *ACS Nano*, 2012, **6**, 8468-8483.
2. K. L. Viola, J. Sbarboro, R. Sureka, M. De, M. A. Bicca, J. Wang, S. Vasavada, S. Satpathy, S. Wu, H. Joshi, P. T. Velasco, K. MacRenaris, E. A. Waters, C. Lu, J. Phan, P. Lacor, P. Prasad, V. P. Dravid and W. L. Klein, *Nat. Nanotechnol.*, 2015, **10**, 91-98.
3. S. Marchesan and M. Prato, *ACS Med. Chem. Letters*, 2013, **4**, 147-149.
4. J. Callejas-Fernández, J. Estelrich, M. Quesada-Pérez and J. Forcada, *Soft Nanoparticles for Biomedical Applications*, Royal Society of Chemistry, 2014.
5. O. S. Wolfbeis, *Chem. Soc. Rev.*, 2015, **44**, 4743-4768.
6. B. Pelaz, C. Alexiou, R. A. Alvarez-Puebla, F. Alves, A. M. Andrews, S. Ashraf, L. P. Balogh, L. Ballerini, A. Bestetti, C. Brendel, S. Bosi, M. Carril, W. C. W. Chan, C. Chen, X. Chen, X. Chen, Z. Cheng, D. Cui, J. Du, C. Dullin, A. Escudero, N. Feliu, M. Gao, M. George, Y. Gogotsi, A. Grünweller, Z. Gu, N. J. Halas, N. Hampp, R. K. Hartmann, M. C. Hersam, P. Hunziker, J. Jian, X. Jiang, P. Jungebluth, P. Kadhiresan, K. Kataoka, A. Khademhosseini, J. Kopeček, N. A. Kotov, H. F. Krug, D. S. Lee, C.-M. Lehr, K. W. Leong, X.-J. Liang, M. Ling Lim, L. M. Liz-Marzán, X. Ma, P. Macchiarini, H. Meng, H. Möhwald, P. Mulvaney, A. E. Nel, S. Nie, P. Nordlander, T. Okano, J. Oliveira, T. H. Park, R. M. Penner, M. Prato, V. Puntes, V. M. Rotello, A. Samarakoon, R. E. Schaak, Y. Shen, S. Sjöqvist, A. G. Skirtach, M. G. Soliman, M. M. Stevens, H.-W. Sung, B. Z. Tang, R. Tietze, B. N. Udugama, J. S. VanEpps, T. Weil, P. S. Weiss, I. Willner, Y. Wu, L. Yang, Z. Yue, Q. Zhang, Q. Zhang, X.-E. Zhang, Y. Zhao, X. Zhou and W. J. Parak, *ACS Nano*, 2017, **11**, 2313-2381.
7. S. Kunjachan, J. Ehling, G. Storm, F. Kiessling and T. Lammers, *Chem. Rev.*, 2015, **115**, 10907-10937.
8. J. Liu, C. Detrembleur, S. Mornet, C. Jerome and E. Duguet, *J. Mat. Chem. B*, 2015, **3**, 6117-6147.
9. J. A. Barreto, W. O'Malley, M. Kubeil, B. Graham, H. Stephan and L. Spiccia, *Adv. Mater.*, 2011, **23**, H18-H40.
10. E. Blanco, H. Shen and M. Ferrari, *Nat Biotech*, 2015, **33**, 941-951.
11. R. Hardman, *Environ. Health Perspect.*, 2006, **114**, 165-172.
12. W. G. Kreyling, A. M. Abdelmonem, Z. Ali, F. Alves, M. Geiser, N. Haberl, R. Hartmann, S. Hirn, D. J. de Aberasturi, K. Kantner, G. Khadem-Saba, J.-M. Montenegro, J. Rejman, T. Rojo, I. R. de Larramendi, R. Ufartes, A. Wenk and W. J. Parak, *Nat. Nanotechnol.*, 2015, **10**, 619-623.
13. K. Pant, O. Sedláček, R. A. Nadar, M. Hrubý and H. Stephan, *Adv. Healthc. Mater.*, 2017, **6**, 1601115.
14. N. Feliu, D. Docter, M. Heine, P. del Pino, S. Ashraf, J. Kolosnjaj-Tabi, P. Macchiarini, P. Nielsen, D. Alloyeau, F. Gazeau, R. H. Stauber and W. J. Parak, *Chem. Soc. Rev.*, 2016, **45**, 2440-2457.
15. X.-D. Zhang, J. Yang, S.-S. Song, W. Long, J. Chen, X. Shen, H. Wang, Y.-M. Sun, P.-X. Liu and S. Fan, *Int. J. Nanomed.*, 2014, **9**, 2069-2072.
16. H. Soo Choi, W. Liu, P. Misra, E. Tanaka, J. P. Zimmer, B. Itty Ipe, M. G. Bawendi and J. V. Frangioni, *Nat. Biotechnol.*, 2007, **25**, 1165-1170.
17. M. Longmire, P. L. Choyke and H. Kobayashi, *Nanomed.*, 2008, **3**, 703-717.
18. B. H. Kim, M. J. Hackett, J. Park and T. Hyeon, *Chem. Mater.*, 2014, **26**, 59-71.
19. K. Zarschler, L. Rocks, N. Licciardello, L. Boselli, E. Polo, K. P. Garcia, L. De Cola, H. Stephan and K. A. Dawson, *Nanomedicine: NBM*, 2016, **12**, 1663-1701.
20. H. M. Smilowitz, L. J. Tarmu, M. M. Sanders, J. A. Taylor, 3rd, D. Choudhary, C. Xue, N. A. Dyment, D. Sasso, X. Deng and J. F. Hainfeld, *Int. J. Nanomed.*, 2017, **12**, 7937-7946.
21. S. Shen, D. Jiang, L. Cheng, Y. Chao, K. Nie, Z. Dong, C. J. Kutyreff, J. W. Engle, P. Huang, W. Cai and Z. Liu, *ACS Nano*, 2017, **11**, 9103-9111.
22. B. R. Smith and S. S. Gambhir, *Chem. Rev.*, 2017, **117**, 901-986.
23. U. Resch-Genger, M. Grabolle, S. Cavaliere-Jaricot, R. Nitschke and T. Nann, *Nat. Meth.*, 2008, **5**, 763-775.
24. A. M. Derfus, W. C. W. Chan and S. N. Bhatia, *Nano. Lett.*, 2004, **4**, 11-18.
25. S. Kim, Y. T. Lim, E. G. Soltesz, A. M. De Grand, J. Lee, A. Nakayama, J. A. Parker, T. Mihaljevic, R. G. Laurence, D. M. Dor, L. H. Cohn, M. G. Bawendi and J. V. Frangioni, *Nat. Biotechnol.*, 2004, **22**, 93-97.
26. W. Liu, H. S. Choi, J. P. Zimmer, E. Tanaka, J. V. Frangioni and M. Bawendi, *J. Am. Chem. Soc.*, 2007, **129**, 14530-14531.
27. C. Chen, P. Zhang, L. Zhang, D. Gao, G. Gao, Y. Yang, W. Li, P. Gong and L. Cai, *Chem. Commun.*, 2015, **51**, 11162-11165.
28. G. Xu, S. Zeng, B. Zhang, M. T. Swihart, K.-T. Yong and P. N. Prasad, *Chem. Rev.*, 2016, **116**, 12234-12327.
29. J. Wang and J. Qiu, *J. Mater. Sci.*, 2016, **51**, 4728-4738.
30. G. Hong, S. Diao, A. L. Antaris and H. Dai, *Chem. Rev.*, 2015, **115**, 10816-10906.

31. M. Rosso-Vasic, E. Spruijt, Z. Popovic, K. Overgaag, B. van Lagen, B. Grandidier, D. Vanmaekelbergh, D. Dominguez-Gutierrez, L. De Cola and H. Zuilhof, *J. Mater. Chem.*, 2009, **19**, 5926-5933.
32. X. Cheng, S. B. Lowe, P. J. Reece and J. J. Gooding, *Chem. Soc. Rev.*, 2014, **43**, 2680-2700.
33. J. H. Warner, A. Hoshino, K. Yamamoto and R. D. Tilley, *Angew. Chem. Int. Ed.*, 2005, **44**, 4550-4554.
34. C. Fu, L. Qiang, T. Liu, L. Tan, H. Shi, X. Chen, X. Ren and X. Meng, *J. Mat. Chem. B*, 2014, **2**, 6978-6983.
35. M. Algarra, M. Perez-Martin, M. Cifuentes-Rueda, J. Jimenez-Jimenez, J. C. G. Esteves da Silva, T. J. Bandosz, E. Rodriguez-Castellon, J. T. Lopez Navarrete and J. Casado, *Nanoscale*, 2014, **6**, 9071-9077.
36. S.-T. Yang, L. Cao, P. G. Luo, F. Lu, X. Wang, H. Wang, M. J. Meziani, Y. Liu, G. Qi and Y.-P. Sun, *J. Am. Chem. Soc.*, 2009, **131**, 11308-11309.
37. S. Ruan, J. Qian, S. Shen, J. Zhu, X. Jiang, Q. He and H. Gao, *Nanoscale*, 2014, **6**, 10040-10047.
38. X. Cheng, S. B. Lowe, S. Ciampi, A. Magenau, K. Gaus, P. J. Reece and J. J. Gooding, *Langmuir*, 2014, **30**, 5209-5216.
39. Z. Peng, X. Han, S. Li, A. O. Al-Youbi, A. S. Bashammakh, M. S. El-Shahawi and R. M. Leblanc, *Coord. Chem. Rev.*, 2017, **343**, 256-277.
40. S. Y. Lim, W. Shen and Z. Gao, *Chem. Soc. Rev.*, 2015, **44**, 362-381.
41. Z. F. Li and E. Ruckenstein, *Nano Lett.*, 2004, **4**, 1463-1467.
42. S. Ohta, P. Shen, S. Inasawa and Y. Yamaguchi, *J. Mater. Chem.*, 2012, **22**, 10631-10638.
43. L. Ruizendaal, S. Bhattacharjee, K. Pournazari, M. Rosso-Vasic, L. H. J. de Haan, G. M. Alink, A. T. M. Marcelis and H. Zuilhof, *Nanotoxicology*, 2009, **3**, 339-347.
44. S. Bhattacharjee, I. M. Rietjens, M. P. Singh, T. M. Atkins, T. K. Purkait, Z. Xu, S. Regli, A. Shukaliak, R. J. Clark, B. S. Mitchell, G. M. Alink, A. T. Marcelis, M. J. Fink, J. G. Veinot, S. M. Kauzlarich and H. Zuilhof, *Nanoscale*, 2013, **5**, 4870-4883.
45. F. Peng, Y. Su, Y. Zhong, C. Fan, S.-T. Lee and Y. He, *Acc. Chem. Res.*, 2014, **47**, 612-623.
46. J.-H. Park, L. Gu, G. von Maltzahn, E. Ruoslahti, S. N. Bhatia and M. J. Sailor, *Nat. Mater.*, 2009, **8**, 331-336.
47. L. T. Canham, *Adv. Mater.*, 1995, **7**, 1033-1037.
48. N. K. Hon, Z. Shaposhnik, E. D. Diebold, F. Tamanoi and B. Jalali, *J. Biomed. Mater. Res. A*, 2012, **100A**, 3416-3421.
49. M. Dasog, Z. Yang, S. Regli, T. M. Atkins, A. Faramus, M. P. Singh, E. Muthuswamy, S. M. Kauzlarich, R. D. Tilley and J. G. C. Veinot, *ACS Nano*, 2013, **7**, 2676-2685.
50. S. N. Baker and G. A. Baker, *Angew. Chem. Int. Ed.*, 2010, **49**, 6726-6744.
51. M. L. Bhaisare, A. Talib, M. S. Khan, S. Pandey and H. F. Wu, *Microchim. Acta*, 2015, **182**, 2173-2181.
52. Z. Fan, S. Li, F. Yuan and L. Fan, *RSC Adv.*, 2015, **5**, 19773-19789.
53. D. Mazzier, M. Favaro, S. Agnoli, S. Silvestrini, G. Granozzi, M. Maggini and A. Moretto, *Chem. Commun.*, 2014, **50**, 6592-6595.
54. M. Montalti, A. Cantelli and G. Battistelli, *Chem. Soc. Rev.*, 2015, **44**, 4853-4921.
55. F. Chen, S. Goel, R. Hernandez, S. A. Graves, S. Shi, R. J. Nickles and W. Cai, *Small*, 2016, **12**, 2775-2782.
56. E. Phillips, O. Penate-Medina, P. B. Zanzonico, R. D. Carvajal, P. Mohan, Y. Ye, J. Humm, M. Gönen, H. Kalaigian, H. Schöder, H. W. Strauss, S. M. Larson, U. Wiesner and M. S. Bradbury, *Sci. Transl. Med.*, 2014, **6**, 260ra149-260ra149.
57. Y. Zhao, D. Sultan, L. Detering, H. Luehmann and Y. Liu, *Nanoscale*, 2014, **6**, 13501-13509.
58. Y. Zhao, L. Detering, D. Sultan, M. L. Cooper, M. You, S. Cho, S. L. Meier, H. Luehmann, G. Sun, M. Rettig, F. Dehdashti, K. L. Wooley, J. F. DiPersio and Y. Liu, *ACS Nano*, 2016, **10**, 5959-5970.
59. M. Zhou, J. Li, S. Liang, A. K. Sood, D. Liang and C. Li, *ACS Nano*, 2015, **9**, 7085-7096.
60. F. Gao, P. Cai, W. Yang, J. Xue, L. Gao, R. Liu, Y. Wang, Y. Zhao, X. He, L. Zhao, G. Huang, F. Wu, Y. Zhao, Z. Chai and X. Gao, *ACS Nano*, 2015, **9**, 4976-4986.
61. Y. Zhong, F. Peng, F. Bao, S. Wang, X. Ji, L. Yang, Y. Su, S.-T. Lee and Y. He, *J. Am. Chem. Soc.*, 2013, **135**, 8350-8356.
62. L. Wang, Y. Wang, T. Xu, H. Liao, C. Yao, Y. Liu, Z. Li, Z. Chen, D. Pan, L. Sun and M. Wu, *Nat. Commun.*, 2014, **5**.
63. K. Dohnalova, A. N. Poddubny, A. A. Prokofiev, W. D. A. M. de Boer, C. P. Umesh, J. M. J. Paulusse, H. Zuilhof and T. Gregorkiewicz, *Light. Sci. Appl.*, 2013, **2**, e47.
64. Y.-P. Sun, B. Zhou, Y. Lin, W. Wang, K. A. S. Fernando, P. Pathak, M. J. Meziani, B. A. Harruff, X. Wang, H. Wang, P. G. Luo, H. Yang, M. E. Kose, B. Chen, L. M. Veca and S.-Y. Xie, *J. Am. Chem. Soc.*, 2006, **128**, 7756-7757.
65. L. Wang, S.-J. Zhu, H.-Y. Wang, S.-N. Qu, Y.-L. Zhang, J.-H. Zhang, Q.-D. Chen, H.-L. Xu, W. Han, B. Yang and H.-B. Sun, *ACS Nano*, 2014, **8**, 2541-2547.
66. S. M. Quadri and H. M. Vriesendorp, *Q. J. Nucl. Med. Mol. Imaging*, 1998, **42**, 250-261.
67. M. S. Cooper, M. T. Ma, K. Sunassee, K. P. Shaw, J. D. Williams, R. L. Paul, P. S. Donnelly and P. J. Blower, *Bioconjug. Chem.*, 2012, **23**, 1029-1039.
68. M. Shokeen and C. J. Anderson, *Acc. Chem. Res.*, 2009, **42**, 832-841.
69. M. D. Bartholomä, *Inorg. Chim. Acta*, 2012, **389**, 36-51.
70. K. Zarschler, M. Kubeil and H. Stephan, *RSC Adv.*, 2014, **4**, 10157-10164.
71. V. Maheshwari, J. L. J. Dearling, S. T. Treves and A. B. Packard, *Inorg. Chim. Acta*, 2012, **393**, 318-323.
72. E. W. Price and C. Orvig, *Chem. Soc. Rev.*, 2014, **43**, 260-290.
73. P. Comba, B. Martin, A. Sanyal and H. Stephan, *Dalton Trans.*, 2013, **42**, 11066-11073.
74. B. Das, P. Dadhich, P. Pal, P. K. Srivas, K. Bankoti and S. Dhara, *J. Mat. Chem. B*, 2014, **2**, 6839-6847.
75. J. H. Ahire, Q. Wang, P. R. Coxon, G. Malhotra, R. Brydson, R. Chen and Y. Chao, *ACS Appl. Mater. Interfaces*, 2012, **4**, 3285-3292.
76. M. Behray, C. A. Webster, S. Pereira, P. Ghosh, S. Krishnamurthy, W. T. Al-Jamal and Y. Chao, *ACS Appl. Mater. Interfaces*, 2016, **8**, 8908-8917.
77. K. Jain, P. Kesharwani, U. Gupta and N. K. Jain, *Int. J. Pharm.*, 2010, **394**, 122-142.
78. S. Bhattacharjee, L. de Haan, N. Evers, X. Jiang, A. Marcelis, H. Zuilhof, I. Rietjens and G. Alink, *Part. Fibre Toxicol.*, 2010, **7**, 25.
79. W. Möller, D. M. Brown, W. G. Kreyling and V. Stone, *Part. Fibre Toxicol.*, 2005, **2**, 7-7.
80. L. Foucaud, M. R. Wilson, D. M. Brown and V. Stone, *Toxicol. Lett.*, 2007, **174**, 1-9.
81. D. Walczyk, F. B. Bombelli, M. P. Monopoli, I. Lynch and K. A. Dawson, *J. Am. Chem. Soc.*, 2010, **132**, 5761-5768.
82. D. F. Moyano, K. Saha, G. Prakash, B. Yan, H. Kong, M. Yazdani and V. M. Rotello, *ACS Nano*, 2014, **8**, 6748-6755.
83. S. Ashraf, J. Park, M. A. Bichelberger, K. Kantner, R. Hartmann, P. Maffre, A. H. Said, N. Feliu, J. Lee, D. Lee, G. U. Nienhaus, S. Kim and W. J. Parak, *Nanoscale*, 2016, **8**, 17794-17800.
84. K. Pombo-García, S. Weiss, K. Zarschler, C.-S. Ang, R. Hübner, J. Pufe, S. Meister, J. Seidel, J. Pietzsch, L. Spiccia, H. Stephan and B. Graham, *ChemNanoMat*, 2016, **2**, 959-971.
85. K. Huang, H. Ma, J. Liu, S. Huo, A. Kumar, T. Wei, X. Zhang, S. Jin, Y. Gan, P. C. Wang, S. He, X. Zhang and X.-J. Liang, *ACS Nano*, 2012, **6**, 4483-4493.
86. A. Z. Ruiz, D. Brühwiler, T. Ban and G. Calzaferri, *Monatsh. Chem.*, 2005, **136**, 77-89.
87. K. Pombo-García, K. Zarschler, J. A. Barreto, J. Hesse, L. Spiccia, B. Graham and H. Stephan, *RSC Adv.*, 2013, **3**, 22443.
88. K. Zarschler, K. Prapainop, E. Mahon, L. Rocks, M. Bramini, P. M. Kelly, H. Stephan and K. A. Dawson, *Nanoscale*, 2014, **6**, 6046-6056.
89. S. Thieme, M. Walther, H. J. Pietzsch, J. Henniger, S. Preusche, P. Mäding and J. Steinbach, *Appl. Radiat. Isot.*, 2012, **70**, 602-608.
90. A. Leonidova, C. Foerster, K. Zarschler, M. Schubert, H.-J. Pietzsch, J. Steinbach, R. Bergmann, N. Metzler-Nolte, H. Stephan and G. Gasser, *Chem. Sci.*, 2015, **6**, 5601-5616.

91. M. Ullrich, R. Bergmann, M. Peitzsch, E. F. Zenker, M. Cartellieri, M. Bachmann, M. Ehrhart-Bornstein, N. L. Block, A. V. Schally, G. Eisenhofer, S. R. Bornstein, J. Pietzsch and C. G. Ziegler, *Theranostics*, 2016, **6**, 650-665.

